Construction and analysis of surface phase diagrams to describe segregation and dissolution behavior of Al and Ca in Mg alloys

K. B. Sravan Kumar, Mira Todorova,* and Jörg Neugebauer
Department for Computational Materials Science, Max-Planck-Institut für Eisenforschung GmbH, Max-Planck-Str. 1, D-40237 Düsseldorf, Germany

(Dated: July 21, 2022)

Segregation and dissolution behavior of Mg alloyed with Ca and Al are studied by performing density functional theory calculations considering an extensive set of surface structures and compositions. Combining a McLean-like approach to describe disordered surface structures with ab initio surface science approaches for ordered surface structures we construct surface phase diagrams for these alloys. We utilize these diagrams to study segregation phenomena and chemical trends for surfaces in contact with a dry environment or with an aqueous electrolyte. We show that the presence of water dramatically impacts the stability and chemical composition of the considered metallic surfaces. We furthermore find that the two alloying elements behave qualitatively different: whereas Ca strongly segregates to the surface and becomes dissolved upon exposure of the surface to water, Al shows an anti-segregation behavior, i.e., it remains in Mg bulk. These findings provide an explanation for the experimentally observed increase/decrease in corrosion rates when alloying Mg with Al/Ca.

I. INTRODUCTION

Magnesium with its very low density of 1.74 g/cm^3 [1] and a price comparable to that of commonly used aluminum alloys shows great promise towards developing lightweight materials in automotive and aerospace industries. Mg and its alloys have also great potential for improving the energy density in batteries as either cathode and anode materials [2], due to the ability of Mg to carry twice as much charge as Li and its lower cost. Other promising applications relate to their use as biodegradable implants, by exploiting the non-toxic nature of Mg, its mechanical properties similar to bones and its ability to corrode easily, which could circumvent the need for implant removal [3].

Despite having applications in such diverse fields, Mg based alloys suffer from two major limitations: poor ductility [4] and poor corrosion resistance [5]. The ductility of Mg can be significantly improved upon alloying with small amounts of the inexpensive and non-toxic Al (1 wt.%) and Ca (0.1 wt.%) [4]. At higher concentrations of a few weight percent, the same alloying elements (Al and Ca) refine the grain size of Mg, thereby improving its mechanical strength [6]. The reduction of the Mg grain sizes is due to the inhibition of the grain boundary motion during re-crystallization by finely dispersed Mg_2Ca particles forming at calcium contents of 2-3 wt. %, as shown by high-ratio differential speed rolling (HRDSR) [7]. Overall, alloying of Mg with Al and Ca improves its mechanical properties.

Alloying with Al and Ca has also an impact on the corrosion properties of Mg. Increasing the Ca content in Mg alloys leads to an increased anodic corrosion potential [8]. This is consistent with the observation that Mg_2Ca has a larger anodic corrosion potential compared to pure Mg indicating that Ca is anodic in Mg alloys [9]. Anodic corrosion potentials imply that metal atoms become oxidized and dissolve in the electrolyte as positively charged metal ions (Mg^{2+}, Ca^{2+}). The corrosion rate becomes significantly higher for Ca concentrations above the solubility limit in Mg [10–12]. In contrast, Mg alloys with 2-10 wt. % Al, as well as Mg-Al intermetallics (Mg_2Al_3, $Mg_{17}Al_{12}$), show an increased cathodic potential compared to Mg, i.e. they are less prone to corrosion [9, 13]. Indeed, the corrosion rates of Mg alloys were found to decrease upon increasing Al content [12, 14]. The anodic nature of Ca in the corrosion experiments points towards a preferential oxidation of Ca, which acts as a sacrificial anode upon exposure to water. In contrast, Al with its cathodic nature is expected to remain in a Mg alloy.

This picture is also confirmed by computations. Electrochemical potentials calculated using a Born-Haber cycle indicate that the Mg-Al intermetallic $Mg_{17}Al_{12}$ is more cathodic than Mg, while the Mg-Ca intermetallic Mg_2Ca is more anodic than Mg [15]. Surface energies of low index Mg surfaces with Al and Ca substituting Mg atoms in the surface layer calculated using density functional theory (DFT) indicate a higher dissolution rate for Ca compared to Al [16]. Similar to the observations in the corrosion experiments, dissolution potential differences, calculated using chemical potentials derived from Mg vacancy formation energies in the presence of Al and Ca substituted in Mg surfaces, show Al to be more cathodic in nature than Ca [16]. While these computational investigations provide a first qualitative understanding of the impact Al and Ca have on Mg corrosion [15, 16] critical questions remain. For example, the surface structures of the Mg alloys, dependencies on the alloy concentration and the impact of water on the surface segregation behavior are less explored.

A step in this direction is provided by a DFT study looking at the segregation behaviour of various alloying

* m.todorova@mpie.de

elements substituting a Mg atom in the first layer for the single coverage of $\frac{1}{9}$ ML (monolayer; at 1 ML all atoms in the topmost Mg layer would be substituted by an alloying element) [17]. This study showed that segregation of Ca from the bulk to the Mg (0001) surface is thermodynamically favored. However, the systematic exploration of the dependence of Al and Ca surface segregation on alloy concentration, as well as the transfer of this information to construct surface phase diagrams, is lacking.

In this study, we therefore employ DFT calculations and focus on the initial, i.e. non-oxidised state of Mg alloys with dilute bulk concentrations of Al and Ca, constructing surface phase and surface Pourbaix diagrams. To identify the stable surface structures, we consider two scenarios: i) the surface of as cast Mg-Al and Mg-Ca alloys in the absence of an oxidizing medium (in vacuum) and ii) the surface when the as cast alloy is exposed to a corrosive environment. Accounting for the relevance of water for wet corrosion we include it in the calculations for the later case, by modelling it as an implicit solvent [18, 19]. The dependence of the surface segregation behavior on surface coverage is accounted for by considering different surface coverages ranging from as low as $\Theta = \frac{1}{36}$ ML up to a full monolayer.

II. METHODS

A. Density functional theory calculations

All DFT calculations are performed in a plane wave based DFT framework and the projector augmented wave (PAW) approach as implemented in the Vienna Ab-initio Simulation Package (VASP) [20, 21]. Exchange and correlation are described with the PBE implementation of the Generalized Gradient Approximation (GGA) [22]. We employ Fermi smearing of 0.1 eV, converge energies to 10^{-5} eV and optimize geometries using a force criterion of 0.01 eV/Å. Based on careful convergence checks we chose an energy cutoff of 360 eV for further calculations, as it ensures that the lattice constants and the cohesive and formation energies of all considered materials are accurate to at least 5×10^{-3} Å and 5 meV each. Surfaces are modelled using six layer thick asymmetric slabs and a vacuum region of 12 Å. For the Mg(0001) (1×1) surface cell we use a $(12 \times 12 \times 1)$ k-point mesh, which is equivalently folded for larger cells. We apply the dipole correction [23] to the electrostatic potential in z-direction for all supercell calculations containing a vacuum region. This set-up ensures that mixing energies for Ca and Al incorporation in the Mg(0001) surface are converged to better than 10 meV per Ca or Al atom. To study the impact of water on the considered surfaces, the vacuum region in the supercell is replaced by a solvent using an implicit solvation model based on Poisson-Boltzmann as implemented in VASPsol [18, 19]. For these calculations we used eight layer thick symmetric slabs to obtain work functions and interface energies, removing the need to apply a dipole correction [23] inside the implicit solvent.

B. Methodologies for constructing surface phase diagrams

To determine the segregation behavior of alloying elements on the surface we combine in the following two concepts: (i) the surface chemistry approach commonly used to construct phase diagrams for reconstructed and/or chemically ordered surfaces [24–26] and (ii) the concept of Langmuir-McLean isotherms [27]. The latter concept has been originally developed to describe segregation at interfaces, and applies when impurity-impurity interaction at the interface can be neglected. We note, that Johansson and Wahnström [28] have used an alternative CALPHAD-derived approach to obtain interfacial phase diagrams for V-doped WC-Co.

Starting point of both approaches we employ is the Gibbs energy necessary to create a surface with a given stoichiometry in a thermodynamically open (grand canonical) setup. For the system considered here, Al and Ca at the Mg(0001) surface, we compute the surface Gibbs energy as

$$G_{\text{surf}} = \frac{1}{2A}(E^{\text{DFT}}_{\text{Mg-X}} - n_{\text{Mg}}\mu_{\text{Mg}} - n_{\text{X}}\mu_{\text{X}} - TS_{\text{surf}}) \quad (1)$$

where $\text{E}^{\text{DFT}}_{\text{Mg-X}}$ is the DFT calculated energy of the X=Al/Ca substituted Mg surface slab. $n_{\text{Mg/X}}$ is the total number of Mg/X atoms, respectively. The chemical potentials μ_{Mg} and μ_{X} describe the chemical reservoirs with which the Mg and X atoms are in equilibrium. The chemical potentials are referenced to Mg hcp bulk (for Mg) and bulk fcc Al/Ca (for Al/Ca). A is the surface area of the respective supercell and the factor two takes into account that we have two equivalent surfaces for a symmetric slab. S is the excess surface entropy. The dominant entropic contribution is configurational entropy. Other contributions such as electronic or vibrational entropy are substantially smaller and will be neglected in this study.

The concentration of the X atoms in bulk is given by c_{X}. The surface concentration (coverage) Θ_{X} describes the ratio between X and Mg atoms in the top or second surface layer. The first describes the surface coverage, the second the subsurface one. The configurational entropy $S(x)$ entering Eq. 1 is:

$$S = -k_{\text{B}}\left[x \cdot lnx + (1-x) \cdot ln(1-x)\right]. \quad (2)$$

At low coverages the interaction between solute atoms X becomes small. In the absence of solute-solute interaction the solutes will be randomly distributed on the surface and the substitution energy E^{X}_b to replace a Mg atom by Al or Ca is a constant. For such a disordered surface Eq. 1 becomes than:

$$G^{\text{disordered}} = G_0 - \Theta(E_b - (\mu_{\text{X}} - \mu_{\text{Mg}})) - TS(\Theta/\Theta_0). \quad (3)$$

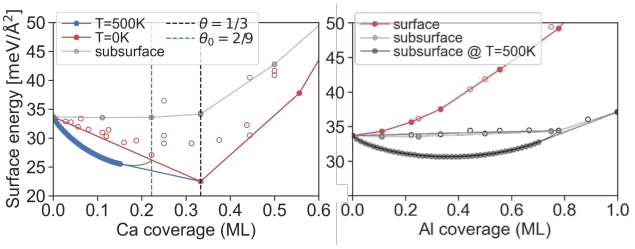

FIG. 1. Surface energies (G_{surf}) upon substitution of (*left*) Ca and (*right*) Al in the Mg(0001) surface and sub-surface layers. Surface energies are calculated in vacuum. The Al/Ca chemical potentials are that of a single Al/Ca atom in Mg bulk. The solid lines show the convex hull construction for the top (red) and subsurface (gray) layer structures at $T = 0\,\mathrm{K}$. The curved blue (for Al) and gray (for Ca) lines show the convex hull at high temperatures ($T = 500\,\mathrm{K}$) due to disorder (Eq. 2).

Here, Θ is the concentration of the solute atoms in the top surface layer and Θ_0 the maximum surface solute concentration up to which solute-solute interaction can be neglected.

1. *Canonical approach in composition space*

The Gibbs energies for the ordered and disordered surfaces depend on both coverage (i.e. chemical composition at the surface/defect) and the chemical potential. In the first approach we use the coverage as state variable, similar to the bulk composition in conventional bulk phase diagrams. We therefore fix the chemical potential. For the following discussion we set it to the energy a single Al/Ca atom would have in bulk Mg at T=0 K. We note, that the convex hull construction we use in the following is invariant to this choice.

Fig. 1 shows the surface energies as function of Ca and Al coverage according to Eq. 1 for solute atoms in the first layer (red) and second layer (gray). The surface energies of the disordered structures at finite temperature ($T = 500\,\mathrm{K}$) computed by Eq. 3 are shown as blue dots (disorder in the first layer) and gray (disorder in the second layer). The thermodynamically stable surface structures are obtained by a convex hull construction (solid lines). These structures are marked by filled dots and lie on the convex hull.

Having a dense set of energies close to the convex hull, such as in the interval between 0 and $\approx 0.22\,\mathrm{ML}$ for Ca, implies that solute-solute interaction is small. In contrast, large gaps between two ordered structures, as e.g. between 0.22 and 0.33 ML for Ca imply a miscibility gap and thus severe solute-solute interactions. For the case of Ca solutes we therefore set $\Theta_0 \approx 0.22$, i.e., to the last structure before the miscibility gap. We note that by construction the surface energy of the ordered and disordered surface, which differ only by the configurational energy $-TS$, are identical at the critical coverage Θ_0 in Eq. 3, where $S(\Theta/\Theta_0) = S(1) = 0$ (Eq. 2).

The filled blue dots in Fig. 1 mark the coverages where the surface is disordered, the straight line between the last blue dot and the 1/3 ordered structure marks a region of phase coexistence between the disordered and the 1/3 ordered structure. The scheme sketched here is reminiscent of the concepts used to construct bulk phase diagrams. It thus can be directly employed in CALPHAD based software tools designed to compute bulk phase diagrams, which allows to extend them to surface or defect phase diagrams. The main difference here is that the chemical concentration is not described by the bulk, but the surface/defect stoichiometry.

2. *Grand-canonical approach in μ space*

A severe limitation of phase diagrams in composition space is that they implicitly assume canonical conditions, i.e., particle conservation. While this is a natural choice for bulk materials, surface and defect structures are often thermodynamically open systems which can exchange atoms with the surrounding host material or with the environment they are in contact with. Therefore, a natural choice for surfaces and defects is to use the chemical potential as state variable for defect phase diagrams (see e.g. [29–31]).

For a binary alloy, we actually have two chemical potentials that enter in the surface energy calculations (Eq. 1). Since we focus here on substitutional surface structures, i.e. structures where a Mg atom is substituted by an Al or Ca atom, only the difference between the chemical potentials of the host and solute species enters in Eqs. 1 and 3.

Fig. 2 shows the chemical potential difference between host and solute chemical potential, as well as the individual host and solute chemical potentials. The latter are given by $\mu = -k_{\mathrm{B}}T \ln x$ with x the concentration of the host/solute in the bulk. As can be seen, up to a solute concentration of $\approx 10\,\%$ the difference in chemical poten-

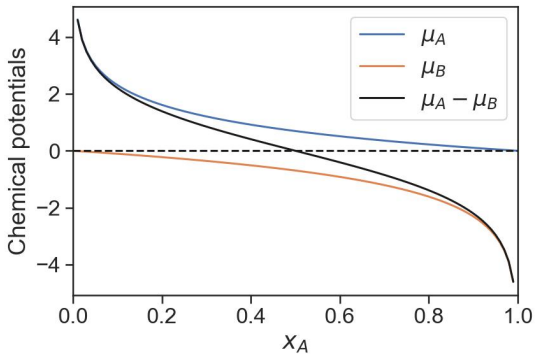

FIG. 2. Difference between the chemical potentials of species A and B in an $\mathrm{A}_{\mathrm{X_A}}\mathrm{B}_{1-\mathrm{X_A}}$ compound. Also shown are the chemical potentials of the two species.

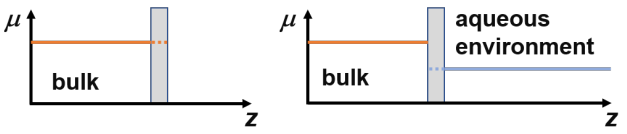

FIG. 3. Chemical potential of the alloying element along the surface normal for the two scenarios considered in the paper: (*left*) The surface is in contact with a dry environment (vacuum). For this case the surface is assumed to be in thermodynamic equilibrium with the bulk. (*right*) The surface is in contact with an aqueous electrolyte. Since adsorption/diffusion kinetics between surface and electrolyte is much faster than diffusion between surface and bulk the surface is assumed to be in thermodynamic equilibrium with the electrolyte.

tials can be safely replaced by the chemical potential of the solute alone, i.e.,

$$(\mu_X - \mu_{Mg}) \approx \mu_X \quad . \tag{4}$$

Since our focus will be on solid solutions and precipitation of Al and Ca occurring at bulk concentrations at about 1 at.% the difference can be safely replaced by the chemical potential of the alloying element alone.

Minimizing the surface Gibbs energy in Eq. 3 with respect to the coverage Θ we obtain the equilibrium surface concentration:

$$\Theta_{eq} = \Theta_0(1 + e^{\Theta_0(E_b - \mu_X)/k_B T})^{-1} \quad . \tag{5}$$

Setting $\Theta = \Theta_{eq}$ in Eq. 3 leaves only μ_X as a free variable, i.e. $G^{\text{disordered}}(\mu_X)$.

The above approach formalizes the well-established equations that are used to describe isotherms in various fields, e.g. Langmuir when the surface is in thermodynamic contact with a gas, Nernst when in contact with an electrolyte, and Langmuir-McLean when in contact with the bulk. It also naturally extends to the surface science approach [32–34] where the Gibbs energies and concentrations are directly expressed as function of chemical potential.

We note that the above expressions are general and do not make any assumption regarding the nature of the chemical reservoir with which the surface interacts. In the following we will discuss two scenarios (see Fig. 3): First, the case when the surface is equilibrated with the bulk alloy composition, i.e., after casting the alloy and before exposing it to an oxygen environment. Second, when the surface gets in contact with a water electrolyte.

3. *Selection of suitable boundary conditions*

Next to a general discussion of chemical trends we select and discuss a few representative bulk alloy compositions. Specifically, we consider in this study bulk mole fractions of 2×10^{-2} and 10^{-3} for Al and Ca respectively,

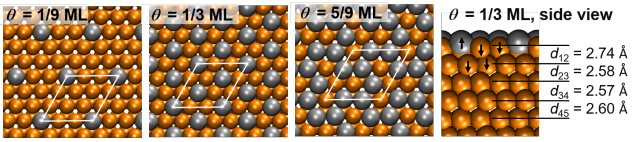

FIG. 4. Surface structures for several coverages of Ca substituting Mg atoms in the surface layer on the Mg(0001) surface shown in top view. The lowest energy structure ($\Theta_{Ca} = 1/3$ ML) is seen also in side view, showing the relaxation pattern. Mg atoms are shown as orange balls, Ca atoms as silver.

mirroring experimentally synthesized solid solutions in these alloys.

To study the scenario when the surface is exposed to an aqueous electrolyte containing ions, chemical potentials for Al^{3+} and Ca^{2+} ions are calculated at the Mg dissolution potential at which Mg dissolves as Mg^{2+}. This dissolution potential is $U = -2.51$ V and calculated from the bulk Mg Pourbaix diagram for a Mg^{2+} concentration of 10^{-5} mol/L, representative of the Mg^{2+} concentrations observed in experiments [35]. The dependence of chemical potentials of Al and Ca on their ion concentrations [36] are given by:

$$\mu_{Al^{3+}} = \Delta G^0_{Al^{3+}} + k_B T \cdot ln\frac{c_{Al^{3+}}}{c_0} + 3(U_{SHE} - U), \tag{6}$$

$$\mu_{Ca^{2+}} = \Delta G^0_{Ca^{2+}} + k_B T \cdot ln\frac{c_{Ca^{2+}}}{c_0} + 2(U_{SHE} - U), \tag{7}$$

where $\Delta G^0_{Al^{3+}}$ and $\Delta G^0_{Ca^{2+}}$ are the formation energies of Al^{3+} and Ca^{2+} ions respectively. For the standard hydrogen electrode potential (U_{SHE}) we chose -4.73 V, similar to previous studies [36], and consider concentrations of $c_{Al^{3+}} = 3 \times 10^{-7}$ and $c_{Ca^{2+}} = 8 \times 10^{-8}$ mol/L, representative of concentrations observed in experiments [35].

III. RESULTS AND DISCUSSION

A. Segregation behavior of Al and Ca at as cast Mg surfaces

To study the surface segregation behavior of Al and Ca in vacuum, the Mg atoms in the top surface and the sub-surface layers of a Mg(0001) slab are systematically substituted with Al and Ca atoms thus realising different surface coverages. An illustration of some of the studied Ca substitutions in the surface and sub-surface layers of Mg are shown in Fig. 4.

1. *Surface phase diagrams of as cast surfaces*

Using the formalism outlined in Sec. II B 2 we construct surface phase diagrams for Al and Ca substitution at the

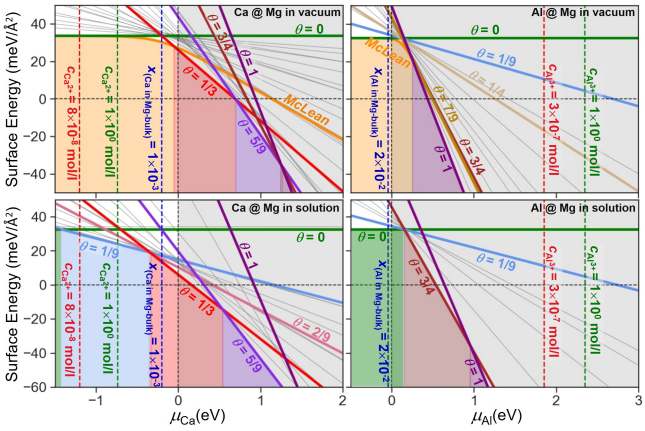

FIG. 5. Surface phase diagrams for Ca and Al substitution at Mg(0001) surfaces *(top)* in vacuum and *(bottom)* in aqueous electrolyte. The surface coverages of Ca and Al are reported in ML. Chemical potentials corresponding to selected Ca/Al concentrations in Mg bulk and different Al^{3+} and Ca^{2+} concentrations in solution are plotted as vertical dashed lines. The dashed black line at $\mu_{Ca/Al} > 0$ marks the solubility limit. The white background to the left marks the region where Ca incorporates as solid solution while to the right precipitates form. The McLean isotherm is calculated for $T = 500\,\mathrm{K}$ in vacuum and $T = 300\,\mathrm{K}$ in solution.

Mg(0001) surface. The unified approach outlined in this section allows us to treat ordered and disordered surfaces in the same framework.

The thus constructed surface phase diagrams are displayed in Fig. 5. Each colored area shows the respective surface phase that has the lowest Gibbs energy for these chemical potentials and that is thus the thermodynamically most stable surface for these conditions. For the surfaces in vacuum, the disordered phases emerge as the most stable ones at low Al/Ca chemical potentials, which correspond to Al/Ca poor conditions (e.g. low Al/Ca concentrations in the bulk). Due to the low chemical potentials the surface solute concentration is low. As a consequence, the interaction between substituted solute atoms at the surface is small and configurational entropy wins over remaining (small) interactions. For Ca, going to higher chemical potentials, a c(3×3) structure with $\Theta = 1/3\,\mathrm{ML}$ coverage and at even higher potentials a structure with a coverage of $\Theta = 5/9\,\mathrm{ML}$ become stable. We also see that already at a temperature of 500 K, as considered here, entropy becomes important and significantly lowers the surface energy compared to the clean surface without segregation (green line with $\Theta = 0$).

For Al segregation a very different behavior is observed. As shown already in Fig. 1, surface structures with Al in the top surface layer are energetically less stable than those with Al in the second layer. The fact that the energy in the second layer remains almost unaffected when increasing the Al coverage, except for extreme high coverages with close to 80 % Al, implies that the solute energy in this layer is close to that in Mg bulk. It also indicates that the solute-solute interaction is small. Al thus shows a strong antisegregation effect on Mg surfaces resulting in Al surface concentrations that are lower than the ones in Mg bulk.

Since for Al the most stable surfaces are the ones in the second layer, which do not show any tendency for ordering, we show for this alloying element a metastable surface phase diagram. This diagram contains exclusively surface structures with Al in the top surface layer. It shows only the disordered phase and a single ordered structure consisting of a full Al monolayer.

Constructing the phase diagram in μ space allows us to include information from the bulk phase diagram, such as phase transitions, in the same diagram. Specifically, the vertical line at zero chemical potential marks the potential at which Ca or Al no longer incorporate as solid solution, but form precipitates. For Ca, as shown in Fig. 5, two surface phases can be realized in the solid solution region ($\mu_{Ca} < 0\,eV$): The random surface structure (a solid solution of Ca and Mg in the top surface layer) and an ordered surface with 1/3 ML Ca coverage. The other ordered surface structures shown in this diagram are thermodynamically unstable. For the meta-stable Al surface phase diagram only the disordered random solution can be formed in the thermodynamically stable region. The meta-stable phases may be formed when going to non-equilibrium conditions where the surface chemical potential can be well above the equilibrium limit.

2. *Segregation isotherms for Ca at the Mg(0001) surface*

The surface phase diagrams can be also directly used to construct segregation isotherms. For any given temperature and chemical potential the most stable surface phase and thus the surface coverage can be deduced. For the disordered surfaces the coverage is given by Eq. 5. To connect to specific experimental scenarios the chemical potential can be expressed by physical quantities that describe the environment with which the surface is in thermodynamic contact. In this section we will consider the initial state of as-cast surfaces, where the solute concentration at the surface and in bulk can be assumed to be in thermodynamic equilibrium (see Fig. 6). In a solid solution, where the Al and/or Ca concentration is low, the Al and Ca chemical potential is $\mu_X = \mu_{X_0} + k_B T \ln x_X$ with X either Al or Ca (see Fig. 2). μ_{X_0} is the energy of a single Al/Ca atom in Mg bulk.

In thermodynamic equilibrium the Al/Ca chemical potential in bulk and at the surface are identical. The chemical potential in the surface energies can thus be substituted by the above expression, allowing us to write it as function of temperature and bulk composition. The resulting segregation isotherms are visualized in Fig. 6 in two representations. In the left diagram (Fig. 6 A) the Ca surface coverage is shown as function of the Ca bulk concentration for a set of temperatures. At low Ca bulk concentrations the surface coverage increases monotonously

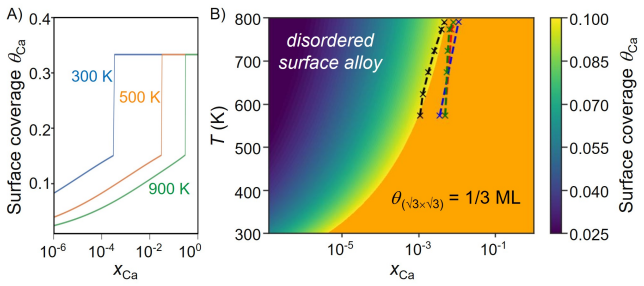

FIG. 6. A.) Surface segregation isotherms at different temperatures for Ca segregation to the Mg(0001) surface. B.) Heat map for coverages of Ca at the Mg(0001) surface at different temperatures and mole fractions of Ca in Mg bulk. Experimentally determined solubility of Ca in Mg bulk taken from Ref. [37]: black line [38], red line [39], blue line [40], green line [41].

until a phase transition to the ordered $\Theta = 1/3$ ML surface structure occurs. This ordered structure pins the coverage, as seen in the appearance of a terrace of constant surface coverage in the plot.

The right diagram (Fig. 6 B) shows a heat map depicting the Ca surface coverage at different temperatures and Ca concentrations in Mg bulk. An increase of the bulk concentration leads to an increase in surface coverage, while an increase in the temperature leads to a decrease in the surface coverage. As a consequence, the bulk Ca concentration required to achieve the Ca surface coverage of $\frac{1}{3}$ ML keeps decreasing with decreasing temperature. Even at bulk Ca concentrations as low as 10^{-5} at. %, when going to sufficiently low temperatures (≈ 300 K) this high surface coverage remains. Of course, at such low temperatures diffusion rates become exceedingly low, preventing the surface from reaching thermodynamic equilibrium/ segregation isotherms in realistic time intervals.

3. *Rationalizing the Al and Ca surface segregation behavior*

To rationalize the strong tendency of Ca to segregate to the Mg surface, as opposed to Al, we consider materials properties like the surface energy or the atomic radii of the involved elements. Looking first at the surface energies of Mg(0001) ($\gamma = 34.7\,\mathrm{meV/Å^2}$), Ca(111) ($\gamma = 34.2\,\mathrm{meV/Å^2}$ [42]) and Al(111) ($\gamma = 41.8\,\mathrm{meV/Å^2}$ [43]) we note, that the surface energies of Mg(0001) and Ca(111) are very similar, while the one of Al is 16 % higher. This suggests that Ca segregation to the surface of Mg will be favorable and possibly even decrease the systems surface energy, while the opposite is expected for Al. Indeed, we find that for the relevant low Ca surface coverage structures (including the 1/3 ML structure, which is reminiscent of a plane in the Mg_2Ca intermetallic) the surface energy is decreased compared to the pristine surface. For Al we observe, as expected, the opposite trend.

The atomic radii of Mg, Ca and Al are 1.60 Å, 1.98 Å and 1.43 Å [1] respectively, showing that Ca is bigger than Mg, while Al is smaller. Consequently, we expect Ca incorporation into the lattice to induce a larger compressive strain, which could be released by segregation to the surface. The release of such unfavorable strain energy would make Ca segregation to the surface energetically highly attractive. To test this hypothesis, we analyse the relaxation behavior of Ca and Al substituted in the Mg surface at different surface coverages. As expected, we find significant outward relaxations for Ca (0.5 - 0.8 Å). For Al, much smaller ($\sim$ 0.2 Å) and inward relaxations are observed. Thus, Ca can release a large part of the compressive strain it has in the bulk at the surface. In contrast, Al, not experiencing large stain in bulk, does not profit from this mechanism.

B. Dissolution behavior of Al and Ca from the Mg surface

To study the dissolution behavior of Al and Ca from the Mg(0001) surface in a corrosive environment we use surface phase diagrams (Fig. 5) constructed from DFT energies. These energies are obtained for coverages of Al and Ca in the top Mg(0001) surface layer. To capture the impact of the electrolyte an implicit solvent approach (VASPsol [18]) is used. This approach emulates an aqueous environment and accounts for its impact on surface structures and energies. We again employ the methodology outlined in section II B, which allows us to treat ordered and disordered structures in the same framework. The diagram (Fig. 5) provides information not only about the surface, but also of the bulk phases.

1. *Impact of solvation on stability and dissolution of the substitutional elements on Mg(0001)*

A comparison of the surface phase diagrams for Al and Ca in the absence and presence of water (Fig. 5) reveals distinct differences. In the following, we will focus only on Ca, since the preference of Al to segregate to the subsurface layer is not changed by the presence of water. As a consequence, the pristine Mg surface is again the dominant phase in the range of chemical potentials compatible with concentrations of bulk solid solution (i.e. $\mu_{Al} < 0$).

The surface phase diagram constructed for Ca substituting Mg atoms in a Mg(0001) surface in contact with water reveals a richer set of ordered phases in the range of chemical potentials compatible with concentrations of bulk solid solution. We see the appearance of a low coverage 1/9 ML Ca ordered phase, which is not found in the absence of water. Modelling an aqueous environment via an implicit solvent provides mainly the electrostatic screening characteristic of the solvent. Thus, the stabilisation of the 1/9 ML structure is related to the built-up

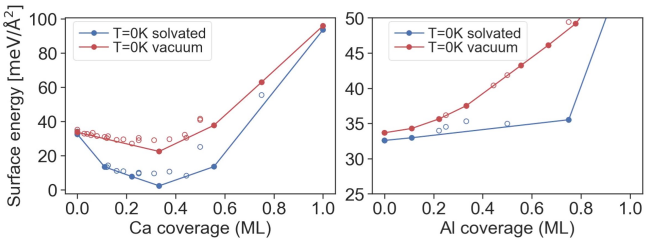

FIG. 7. Surface energies (G_{surf}) upon substitution of (*left*) Ca and (*right*) Al in the Mg(0001) surface in the absence and presence of implicit water.

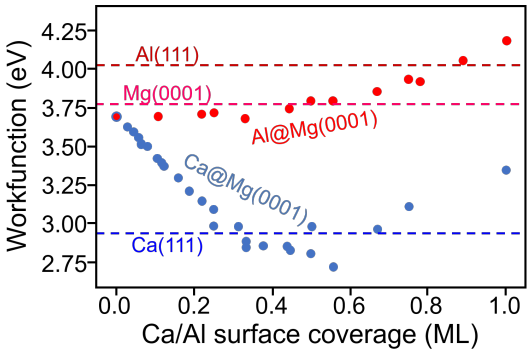

FIG. 8. Impact of Ca/Al substitution on the work function of the Mg(0001) surface. Values for the work functions of the pristine Mg(0001) [45], Al(111) [43] and Ca(111) [42] are marked by dashed lines.

of a partial solvation shell around the Ca atom, which due to its larger size sticks out of the surface layer (see Fig. 4). This stabilisation of Ca surface atoms is absent in the vacuum case. The solvation energy gain is apparently sufficient to overcome the impact of entropy, which is shaping the surface landscape in vacuum at low chemical potentials and favoring disordered surfaces.

The screening of unfavorable electrostatic interactions and the ensuing gain in solvation energy, is an important stabilization mechanism for semiconductor/insulator surfaces in aqueous environment [44]. For metals, it was considered to be of significantly lesser importance due to their large dielectric screening. The appearance of a solvation stabilized Ca structure is therefore significant, since it reveals an efficient solution induced mechanism to stabilize specific surface structures. We finally note, that the presence of the solvent substantially lowers the surface energy (Fig. 7) of Ca substited in the Mg surface, pointing towards a notable energy gain by solvation.

To discuss realistic experimental scenarios we consider a few selected chemical potentials (see Sec. II B 3) that represent bulk (blue dashed lines) or solution concentrations in the electrolyte (dashed red and green lines in Fig. 5). The low concentrations are consistent with experimental observations [35]. For Ca we note that under these conditions surfaces with low Ca coverage are the thermodynamically stable ones. In contrast, for Al even small ion concentrations result in high Al chemical potentials. Under these conditions the 1 ML Al surface structure is the thermodynamically most stable one.

These observations reveal a significantly higher thermodynamic stability of Ca^{2+} ions in solutions, as compared to Ca in Mg bulk. In contrast, for Al the opposite behavior is found: Al^{3+} ions in solution are highly unfavorable compared to substitutional Al in Mg bulk. The higher energetic stability of Ca^{2+} ions in water compared to Ca atoms in Mg bulk favors the dissolution of Ca from the Mg surfaces and prevents the formation of surface structures with higher Ca coverage. A much lower propensity to dissolve is found for Al. A consequence of the higher dissolution tendency of Ca is that under corrosive conditions Al enrichment at the surface occurs.

2. *Impact of Al and Ca segregation on Mg(0001) in the context of micro galvanic corrosion*

The opposite dissolution tendencies of Ca and Al, together with the Al/Ca coverages obtained from the computed surface phase diagrams and the computed electrode potential (work function) of these structures, have direct implications for the corrosion behavior of Mg upon alloying with these elements. To discuss these relations we compute the work functions for the various surface structures and coverages (Fig. 8), since the work function indicates the ease for removing electrons from the surface of a material. For the Mg(0001) surface it increases with increasing coverage of Al and shows the opposite trend (i.e. it decreases) for Ca substitution up to ca. 0.6 ML. From the phase diagrams we know that Al favors high coverages on Mg, while the favorable coverages for Ca lie right within the range of work function decrease. The increase of the work function in the presence of Al means that Al impairs the withdrawal of electrons from Mg, which makes it harder to oxidize the Mg surface. In contrast, the lower work functions for Ca containing surfaces indicates that Ca makes the withdrawal of electrons from the Mg surface easier and therefore promotes its oxidation.

In the context of micro galvanic corrosion these trends in the work functions indicate that Ca is likely to act as anode promoting the electron withdrawal, while Al is likely to act as cathode on the Mg surface, in good agreement with observations of corrosion experiments mentioned in the introduction, i.e Mg shows anodic potentials in the presence of Ca and cathodic potentials in the presence of Al [8, 9, 13]. Here, the anodic nature of Ca implies that Ca prefers to oxidize to Ca^{2+} and dissolve from the Mg surface into the elctrolyte, whereas Al prefers to remain in the Mg surface. This dissolution propensity and the anodic nature of Ca in Mg surfaces provides support to the experimental observations of higher corrosion rates when the Ca content in Mg alloys is increased [10–12].

IV. CONCLUSIONS

Based on an unified thermodynamic approach that allows us to treat ordered and disordered surface structures in the same framework, and by using chemical potentials as state variables, we construct phase diagrams for Mg surfaces alloyed with Al/Ca including bulk information in the same diagram. For Ca we find a strong tendency to segregate to the surface, as opposed to Al which shows an anti-segregation behavior, preferring to remain in a more bulk like environment. Generating surface segregation isotherms we predict the surface coverage expected for a given bulk concentration and temperature. Accounting for realistic environmental conditions suggested by experiment we identify the relevant surface coverage regimes. Comparing surface phase diagrams for initial state of pristine as cast alloys, i.e. surfaces in vacuum, with ones in contact with an aqueous environment, we find that the built up of a partial solvation shell around the protruding Ca atoms at the surface leads to the stabilisation of a low coverage ordered structure absent in vacuum. Furthermore we expect, based on the significantly higher thermodynamic stability of Ca^{2+} ions in solution as opposed to Mg bulk, but also to Al^{3+} ions in solution, and the resulting higher dissolution tendency of Ca, that an Al enrichment at the surface will occur under corrosive conditions. Invoking finally materials properties (like the work function) of all involved elements we rationalise the impact of Al and Ca alloying in Mg in the context of micro-galvanic corrosion and conclude that Ca/Al will be anodic/cathodic in Mg, i.e. the presence of Ca will promote corrosion and Al suppress it.

ACKNOWLEDGMENTS

We acknowledge funding by the Deutsche Forschungsgemeinschaft (DFG, German Research Foundation) through SFB1394, project no. 409476157.

[1] C. Kittell, *Introduction to solid state physics*, Vol. 8 (John Wiley & Sons, Inc., 2005).
[2] R. Van Noorden, The rechargeable revolution: A better battery, Nature News **507**, 26 (2014).
[3] F. Witte, N. Hort, C. Vogt, S. Cohen, K. U. Kainer, R. Willumeit, and F. Feyerabend, Degradable biomaterials based on magnesium corrosion, Current Opinion in Solid State and Materials Science **12**, 63 (2008).
[4] S. Sandlöbes, M. Friák, S. Korte-Kerzel, Z. Pei, J. Neugebauer, and D. Raabe, A rare-earth free magnesium alloy with improved intrinsic ductility, Scientific Reports **7**, 1 (2017).
[5] Y. Yang, F. Scenini, and M. Curioni, A study on magnesium corrosion by real-time imaging and electrochemical methods: Relationship between local processes and hydrogen evolution, Electrochimica Acta **198**, 174 (2016).
[6] Y. C. Lee, A. K. Dahle, and D. H. Stjohn, The role of solute in grain refinement of magnesium, Metallurgical and Materials Transactions A: Physical Metallurgy and Materials Science **31**, 2895 (2000).
[7] J. W. Seong and W. J. Kim, Development of biodegradable Mg-Ca alloy sheets with enhanced strength and corrosion properties through the refinement and uniform dispersion of the Mg2Ca phase by high-ratio differential speed rolling, Acta Biomaterialia **11**, 531 (2015).
[8] N. T. Kirkland, M. P. Staiger, D. Nisbet, C. H. Davies, and N. Birbilis, Performance-driven design of biocompatible Mg alloys, JOM **63**, 28 (2011).
[9] A. D. Südholz, N. T. Kirkland, R. G. Buchheit, and N. Birbilis, Electrochemical properties of intermetallic phases and common impurity elements in magnesium alloys, Electrochemical and Solid-State Letters **14**, 2010 (2011).
[10] N. T. Kirkland, N. Birbilis, J. Walker, T. Woodfield, G. J. Dias, and M. P. Staiger, In-vitro dissolution of magnesium-calcium binary alloys: Clarifying the unique role of calcium additions in bioresorbable magnesium implant alloys, Journal of Biomedical Materials Research - Part B Applied Biomaterials **95**, 91 (2010).
[11] M. S. Syaza Nabilla, C. D. Zuraidawani, and D. M. Nazree, Effect of Ca content percentage and sintering temperature on corrosion rate in Mg-Ca composite fabricated using powder metallurgy technique, AIP Conference Proceedings **1756**, 030009 (2016).
[12] K. Gusieva, C. H. Davies, J. R. Scully, and N. Birbilis, Corrosion of magnesium alloys: The role of alloying, International Materials Reviews **60**, 169 (2015).
[13] L. G. Bland, L. C. Scully, and J. R. Scully, Assessing the corrosion of multi-phase Mg-Al alloys with high al content by electrochemical impedance, mass loss, hydrogen collection, and inductively coupled plasma optical emission spectrometry solution analysis, Corrosion **73**, 526 (2017).
[14] G. Song and A. Atrens, Understanding magnesium corrosion. A framework for improved alloy performance, Advanced Engineering Materials **5**, 837 (2003).
[15] K. Thekkepat, H.-S. Han, J.-W. Choi, S.-C. Lee, E. S. Yoon, G. Li, H.-K. Seok, Y.-C. Kim, J.-H. Kim, and P.-R. Cha, Computational design of Mg alloys with minimal galvanic corrosion, Journal of Magnesium and Alloys https://doi.org/10.1016/j.jma.2021.06.019 (2021).
[16] M. Nezafati, K. Cho, A. Giri, and C. S. Kim, DFT study on the water molecule adsorption and the surface dissolution behavior of Mg alloys, Materials Chemistry and Physics **182**, 347 (2016).
[17] C. Wang, J. Wang, D. Ma, S. Zhu, L. Wang, and S. Guan, First-principles studies on structure stability, segregation, and work function of Mg doped with metal elements, International Journal of Quantum Chemistry **121**, 1 (2021).
[18] K. Mathew, R. Sundararaman, K. Letchworth-Weaver, T. A. Arias, and R. G. Hennig, Implicit solvation model for density-functional study of nanocrystal surfaces and reaction pathways, Journal of Chemical Physics **140**,

https://doi.org/10.1063/1.4865107 (2014).
[19] K. Mathew, V. S. Kolluru, S. Mula, S. N. Steinmann, and R. G. Hennig, Implicit self-consistent electrolyte model in plane-wave density-functional theory, Journal of Chemical Physics **151**, https://doi.org/10.1063/1.5132354 (2019).
[20] G. Kresse and J. Hafner, Ab initio molecular dynamics for liquid metals, Physical Review B **47**, 558 (1993).
[21] G. Kresse and J. Furthmüller, Efficient iterative schemes for ab initio total-energy calculations using a plane-wave basis set, Physical Review B **54**, 11169 (1996).
[22] J. P. Perdew, K. Burke, and M. Ernzerhof, Generalized gradient approximation made simple, Physical Review Letters **77**, 3865 (1996).
[23] J. Neugebauer and M. Scheffler, Adsorbate-substrate and adsorbate-adsorbate interactions of Na and K adlayers on Al(111), Physical Review B **46**, 16067 (1992).
[24] R. Di Felice, J. E. Northrup, and J. Neugebauer, Energetics of AlN thin films and the implications for epitaxial growth on SiC, Physical Review B **54**, R17351 (1996).
[25] J. Neugebauer, T. Zywietz, M. Scheffler, J. E. Northrup, and C. G. Van de Walle, Clean and As-Covered Zinc-Blende GaN (001) Surfaces: Novel Surface Structures and Surfactant Behavior, Physical Review Letter **80**, 3097 (1998).
[26] C. G. Van de Walle and J. Neugebauer, First-Principles Surface Phase Diagram for Hydrogen on GaN Surfaces, Physical Review Letter **88**, 066103 (2002).
[27] D. McLean, *Grain boundaries in metals* (Oxford at the Clarendon Press, 1957) p. 347.
[28] S. A. E. Johansson and G. Wahnström, First-principles study of an interfacial phase diagram in the v-doped wc-co system, Phys. Rev. B **86**, 035403 (2012).
[29] J. Cahn, Transitions and phase equilibria among grain boundary structures, J. Phys. Colloques **43**, C6 (1982).
[30] T. Frolov and Y. Mishin, Phases, phase equilibria, and phase rules in low-dimensional systems, J. Chem. Phys. **143**, 044706 (2015).
[31] S. Korte-Kerzel, T. Hickel, L. Huber, D. Raabe, S. Sandlöbes-Haut, M. Todorova, and J. Neugebauer, Defect phases – thermodynamics and impact on material properties, International Materials Reviews **67**, 89 (2022).
[32] G.-X. Qian, R. Martin, and D. Chadi, First-principles study of the atomic reconstructions and energies of ga- and as-stabilized gaas(100) surfaces, Phys. Rev. B **36**, 7649 (1988).
[33] R. D. Felice, J. E. Northrup, and J. Neugebauer, Energetics of aln thin films and the implications for epitaxial growth on sic, Phys. Rev. B **54**, R17351 (1996).
[34] C. G. Van de Walle and N. J., First-principles surface phase diagram for hydrogen on gan surfaces, Phys. Rev. Lett. **88**, 066103 (2002).
[35] J. Nowak and D. Zander, private communication (2022).
[36] M. Todorova and J. Neugebauer, Extending the concept of defect chemistry from semiconductor physics to electrochemistry, Physical Review Applied **1**, 1 (2014).
[37] A. A. Nayeb-Hashemi and J. B. Clark, The Ca-Mg (Calcium-Magnesium) System, Bulletin of Alloy Phase Diagrams **8**, 58 (1987).
[38] H. Volsskuhler, Der aufbau der magneslumreichen magnesium-kalzium-leglerungen (the phase diagram of magnesium- rich mg-cal alloys), Z. Metallkunde **29**, 236 (1937).
[39] H. Nowotny, E. Wormnes, and A. Mohrnheim, Investigation on the al–ca, mg–ca, and mg–zr systems, Z. Metallkunde **32**, 39 (1940).
[40] J. Haughton, Alloys of magnesium. part vi.-the constitution of the magnesium-rich alloys of magnesium and calcium, J. Inst. Metals **61**, 241 (1937).
[41] W. Bulian and E. Fahrenhorst, The solid solubility of calcium in magnesium, J. Inst. Metals **1**, 70 (1946).
[42] J. Wang and S. Q. Wang, Surface energy and work function of fcc and bcc crystals: Density functional study, Surface Science **630**, 216 (2014).
[43] N. E. Singh-Miller and N. Marzari, Surface energies, work functions, and surface relaxations of low-index metallic surfaces from first principles, Physical Review B - Condensed Matter and Materials Physics **80**, 1 (2009).
[44] S. H. Yoo, M. Todorova, and J. Neugebauer, Selective Solvent-Induced Stabilization of Polar Oxide Surfaces in an Electrochemical Environment, Physical Review Letters **120**, 66101 (2018).
[45] S.-T. Cheng, *A density functional theory study on the oxidation behavior of Mg and Mg-Zn alloys*, Ph.D. thesis, Ruhr-Universität Bochum (2015).